Applied Clay Science 192 (2020) 105638

Contents lists available at ScienceDirect

Applied Clay Science

journal homepage: www.elsevier.com/locate/clay

Research paper

Strong adsorption of phosphate from aqueous solution by zirconium-loaded Ca-montmorillonite

Yinhong Zou[a,b], Runyu Zhang[a,*], Liying Wang[a], Ke Xue[a,b], Jingan Chen[a]

[a] State Key Laboratory of Environmental Geochemistry, Institute of Geochemistry Chinese Academy of Sciences, Guiyang 550081, China
[b] University of Chinese Academy of Sciences, Beijing 100049, China

ARTICLE INFO

Keywords:
Surface water
Eutrophication
Ca-montmorillonite
Zirconium
Modification
Phosphate adsorption

ABSTRACT

Achieving ultralow levels of phosphorus (P) concentrations to prevent eutrophication is an important goal of surface water management. Hence, a highly efficient and economical adsorbent for phosphate removal is urgently required to meet the increasingly stringent water quality standards. This study investigated the phosphate adsorption performance of zirconium (Zr)-modified calcium-montmorillonite (Zr-CaMs). Batch experiments were conducted to obtain the adsorption isotherms, kinetics, and the influences of dosage, solution pH, and coexisting anions. The results demonstrated that Zr was successfully introduced to the surface and interlayer of raw CaM in the presence of the [Si−O]…[HO−Zr≡] hydrogen bond and that it increased the specific surface area. The adsorption isotherms obeyed the Langmuir nonlinear model. The calculated maximum phosphate adsorption capacity was 22.37 mg/g, which was more than twice that of Phoslock. The Elovich model fit the kinetics data well, which was indicative of chemical adsorption. An optimum dosage of 100/1–150/1 and wide pH range (4–8.5) are recommended for practical applications. The coexistence of HCO_3^- slightly inhibited the adsorption capacity, whereas Cl^- and SO_4^{2-} had a positive impact. The adsorption mechanism was primarily the ligand exchange between the surface hydroxyl groups and phosphate resulting from the formation of inner-sphere coordination complexes. This study demonstrated that Zr-CaMs can serve as a prospective adsorbent for phosphate removal from contaminated surface water.

1. Introduction

Since the industrial revolution, the phosphorus (P) cycle has been massively altered by anthropogenic activities (Peñuelas et al., 2012; Koppelaar and Weikard, 2013). P flow has been migrated from the ground to the surface, from the basin to the catchment, resulting in global surface water enrichment and subsequent eutrophication (Smil, 2000; Maavara et al., 2015). Studies have demonstrated that P concentrations above 0.02 mg/L can accelerate water eutrophication and algae propagation (Heathwaite and Sharpley, 1999; Copetti et al., 2016). Thus, the United States Environmental Protection Agency set the stringent limit of total P (TP) 0.05 mg/L for inflowing rivers (Loganathan et al., 2014). China also defines a cut-off TP below this threshold as safe for natural lakes and reservoirs (EQSSW, 2002). However, traditional techniques, such as chemical precipitation and biological treatments, do not easily satisfy such stringent discharge requirements (Loganathan et al., 2014; Wu et al., 2020).

Sorption is a preferable approach for phosphate removal due to its simple design, high performance and efficiency even at low P concentrations, and great potential for resource recovery (Loganathan et al., 2014; Wu et al., 2020). Currently, clay minerals are the most commonly used and effective adsorbents for pollutant removal in contaminated surface waters (Wendling et al., 2013; Gan et al., 2016). Of these minerals, montmorillonite is one of the most promising candidates due to its abundance, low cost, large specific surface area (SSA), and structural adjustability (Huang et al., 2015; Pandey, 2017). It belongs to a typical 2:1 cationic layered silicate clay, with its greater negative surface charge preventing an affinity towards phosphate (Wendling et al., 2013; Huang et al., 2015). To improve its phosphate removal performance, a series of metals, such as iron (Fe), aluminum (Al), lanthanum (La), or mixed La/Al and Zr/Al, have been employed to modify raw montmorillonite (Borgnino et al., 2009; Tian et al., 2009; Huang et al., 2015; Wu et al., 2020). In particular, La-doped bentonite, commercially known as Phoslock, was invented by the Australian Commonwealth Scientific and Industrial Research Organisation to trap phosphate from aqueous solutions in the mid-1990s (Haghseresht et al., 2009). It has undergone extensive development and testing at the laboratory, mesocosm, and even field scale (Robb et al., 2003; Ross et al.,

* Corresponding author.
E-mail address: zhangrunyu@vip.gyig.ac.cn (R. Zhang).

https://doi.org/10.1016/j.clay.2020.105638
Received 16 January 2020; Received in revised form 18 April 2020; Accepted 21 April 2020
Available online 28 April 2020

2008; Spears et al., 2013; Copetti et al., 2016). However, beyond 15,000 RMB/ton, it is economically impracticable for removing phosphate (Marquez-Pacheco et al., 2013; Reitzel et al., 2013a). Moreover, the removal rate is undesirable for certain water bodies and under certain conditions, such as at ultralow P concentrations or in alkaline and saline waters (Ross et al., 2008; Reitzel et al., 2013a; Dithmer et al., 2016), because of its moderate P adsorption capacity of 9.5–10.5 mg/g (Haghseresht et al., 2009; Zamparas et al., 2015). Additionally, high concentrations of leaching La^{3+} may cause potential ecological risks to benthic organisms (Reitzel et al., 2013b; Spears et al., 2013; Copetti et al., 2016). Therefore, a substantial research effort should be devoted to finding an economical P adsorbent with both high recovery efficiency and environmental safety (Copetti et al., 2016; D'Haese et al., 2019).

Zirconium (Zr) is the fourth transition metal, with an abundance of 0.016% in the rocks forming the earth's crust (Wu et al., 2020). Previous studies confirmed that Zr oxides are chemical stable, non-toxic, low water solubility, well resistant to acids/bases and strongly adsorption of phosphate (Chitrakar et al., 2006; Rodrigues et al., 2012; Su et al., 2013). Although Zr-pillared montmorillonite was synthesized using $ZrOCl_2{\cdot}8H_2O$ as the pillaring agent nearly forty years ago (Yamanaka and Brindley, 1979), it has recently regained attention in the pollution remediation field. Zr-modified natural minerals, such as montmorillonite, bentonite, and zeolite have been utilized for phosphate removal from simulated wastewater with high P concentrations (Huang et al., 2015; Zhan et al., 2017; Lin et al., 2018). The maximum phosphate adsorption capacities were 13.1 mg/g for Zr-pillared montmorillonite and 17.2 mg/g for Zr/Al-pillared, respectively (Huang et al., 2015). Recently, Lin et al. (2018) prepared a Zr-loaded bentonite composite and found that its efficient in phosphate removal. Based on their dominant exchangeable cations, natural montmorillonites can be categorized into three types: Na-based montmorillonites, Ca-based montmorillonites, and Mg-based montmorillonites (Zhang et al., 1990; Lin et al., 2018). Currently, China ranks first in the world in terms of proven reserves of montmorillonite (approximately 5 billion tons), and Ca-montmorillonite (CaM) accounts for more than 90% of those reserves. To the best of our knowledge, there has not yet been an exploratory study on phosphate removal from polluted surface water using Zr-modified CaM. Therefore, this study attempted to synthesize a series of Zr-loaded CaMs (Zr-CaMs) through a hydrothermal method and then characterize their chemical compositions and surface morphologies. Phosphate adsorption performances and mechanisms were also investigated by combing batch experiments with isothermal and kinetic models.

2. Materials and methods

2.1. Materials

The raw CaM used in this study was purchased from Ningcheng County, Inner Mongolia Autonomous Region, China. Phoslock was supplied by the Beijing branch of the Phoslock Company in China for a comparative study. Chemical reagents including zirconium oxychloride octahydrate ($ZrOCl_2{\cdot}8H_2O$, purity of 99.0%), potassium dihydrogen phosphate (KH_2PO_4), sodium hydroxide (NaOH), hydrochloric acid (HCl), bicarbonate ($NaHCO_3$), sodium chloride (NaCl), sodium sulfite (Na_2SO_4), potassium antimony tartrate ($C_8H_4K_2O_{12}Sb_2$), ammonium molybdate ($H_8MoN_2O_4$), and ascorbic acid ($C_6H_8O_6$) were all obtained from Shanghai Sinopharm Chemical Reagent Co., Ltd., and they were all analytical grade. Deionized water was used to prepare all the solutions in the experiment.

2.2. Preparation of Zr-CaMs

The raw CaM was modified using different addition amounts of $ZrOCl_2{\cdot}8H_2O$ with the mass ratios of 0.1, 0.5, and 1 to CaM, respectively, based on previous studies (Huang et al., 2015; Lin et al., 2018). These solutions were horizontally shaken in conical flasks for 1 h at 25 °C and 160 rpm. Afterwards, the mixtures were adjusted to a pH of 10.0 with 1 mol/L of NaOH solution, and they reacted for 24 h. The precipitate was separated from the slurry using centrifugation and then rinsed repeatedly with deionized water until there was no Cl in the supernatant as determined by an $AgNO_3$ test, and a circumneutral condition was achieved. The solid products were oven dried at 105 °C and then crushed to a 0.15 mm particle size with a mortar. A series of Zr-CaMs were produced, namely, the adsorbents Zr-CaM0.1, Zr-CaM0.5, and Zr-CaM1.

2.3. Determination of physicochemical properties of raw CaM, Zr-CaMs, and Phoslock

The basic physio-chemical properties of raw CaM and Phoslock, such as the pH value, SSA, cation exchange capacity (CEC), anion exchange capacity (AEC), and TP content, were determined using standard procedures (Zhang et al., 1990; Ruban et al., 2001), and more detailed information can be found in the Supplementary Content Text S1.

The phase structures of raw CaM, Zr-CaMs, and Phoslock were characterized using X-ray diffraction (XRD, Empyream, Panalytical B. V) with Cu-Kα radiation of 40 kV and 20 mA. Their particle surface morphology was studied using scanning electron microscopy (SEM, JSM-7800F, JEOL) at 5 kV. The main chemical compositions of these materials were determined by X-ray fluorescence spectrometry (XRF, Axios PW4400, Empyream, Panalytical B. V). The trace element contents were measured by inductively coupled plasma (ICP) mass spectrometry (ELAN DRC-e, Perkin Elmer) followed by digestion with mixed hydrofluoric acid and nitric acid.

2.4. Batch adsorption tests

Adsorption experiments were carried out to compare the phosphate removal by Zr-CaMs with Phoslock. Potassium dihydrogen phosphate was used to prepare 50 mg P/L stock solution. The initial solution was then diluted to three different P concentration gradients of 0.05 mg/L, 0.1 mg/L, and 0.2 mg/L to stimulate Class III, IV, and V, P thresholds, respectively, for lakes and reservoirs in China (GB3838-2002). Experiments were conducted in duplicate in a water bath shaker at 160 rpm and at a constant temperature of 25 °C to investigate phosphate adsorption as a function of the initial P concentration and contact time. After a certain reaction time, the supernatant was filtered, and then the P concentration was determined by the ascorbic acid method with a detection limit of 0.01 mg/L (APHA, 2017).

2.4.1. Static adsorption experiment

The adsorbent dosage was fit to the mass ratio of 100/1 of adsorbent to TP content in the aqueous solution, which is the recommended ratio for Phoslock (Reitzel et al., 2013a). Different dosages (7.5 mg, 15 mg, and 30 mg) of adsorbents were successively added to the simulated solutions. After stirring for 1 h, the P concentration in the solution was monitored at different intervals until the adsorption equilibrium was reached.

2.4.2. Adsorption isotherm experiment

The initial P concentration range of 1–50 mg/L was set for the isotherm study, with a volume of 50 mL and adsorbent dosage of 25 mg/L. An oscillation experiment was performed for 24 h, and the adsorption capacity at equilibrium was calculated according to the following formula:

$$q_e = \frac{(c_0 - c_e) \times V}{m} \quad (1)$$

where q_e represents the equilibrium adsorption capacity, mg/g; c_0 and

c_e are the P concentrations before and after the adsorption process, respectively, mg/L; V is the solution volume, L; and m is the quality of adsorbents, g.

The experimental data were fitted using three nonlinear isotherm models, including the Langmuir, Freundlich, and Dubinin–Radushkevich (D–R) models (Langmuir, 1916; Freundlich, 1926; Lin et al., 2018). Their specific equations are expressed in the Supplementary Content Text S2.

In addition to determining the correlation coefficient (R^2), mean relative error (MRE) and normalized standard deviation (Δq) were also employed to determine the best-fitting model using Eqs. (2) and (3) (Yazdani et al., 2017; Lin et al., 2018).

$$MRE = \frac{100}{n}\sum\left|\frac{q_{e,cal} - q_{e,\exp}}{q_{e,\exp}}\right| \quad (2)$$

$$\Delta q = \sqrt{\frac{\sum[(q_{e,\exp} - q_{e,cal})/q_{e,\exp}]^2}{n-1}} \quad (3)$$

where $q_{e,cal}$ and $q_{e,\exp}$ are the calculated equilibrium uptake and theoretical adsorbate value, respectively, (mg/g). n represents the number of data points.

2.4.3. Adsorption kinetics experiment

Batch experiments were performed by mixing 30 mg of adsorbent with 1.5 L of phosphate solution with an initial P concentration of 0.2 mg/L for reaction times ranging from 30 min to 4320 min. The kinetic data were further fitted with three typical nonlinear kinetic models (pseudo-first-order, pseudo-second-order, and Elovich models) and an intraparticle diffusion linear model using Origin software (Ho and McKay, 1999; Choi et al., 2016; Lin et al., 2018). The corresponding formulas can be found in the Supplementary Content Text S3.

2.4.4. Effects of influencing factors on phosphate adsorption

Parallel experiments were conducted in a water bath shaker at 160 rpm and at a constant temperature of 25 °C to investigate the influence of adsorbent dosage, solution pH, and coexisting anions on phosphate adsorption, and the detailed experimental procedures can be seen in Supplementary Content Text S4.

3. Results and discussion

3.1. Sample characterizations

Selected properties of raw CaM and Phoslock are listed in Table 1. The pH value of both materials was close to neutral. The SSA and total micropore volume of CaM were twice those of Phoslock. The measured SSA and micropore volume of Phoslock were consistent with those (39.3 m^2/g and 0.171 cc/g) claimed by the manufacturer (Haghseresht et al., 2009). Accordingly, the CEC and AEC of CaM were significantly higher than those of Phoslock, suggesting the superior surface adsorption properties of CaM. This is probably due to the higher purity of montmorillonite than bentonite, which is supported by their respective ethylene blue adsorptions of 49 g/100 g and a little amount. The TP content in CaM was slightly lower than that in Phoslock (Table 1). Hence, the original montmorillonite appeared to pose a lower risk of P release to the ambient environment than that of Phoslock when dissolved in water.

Table 1
Basic physio-chemical properties of raw CaM and Phoslock.

Physico-chemical properties	CaM	Phoslock
pH	7.9	7.2
Specific surface area (m^2/g)	78	39
Micropore volume (cc/g)	0.18	0.09
CEC (mmol 100/g)	117	85
AEC (mmol 100/g)	0.58	0.09
P (mg/kg)	384	491

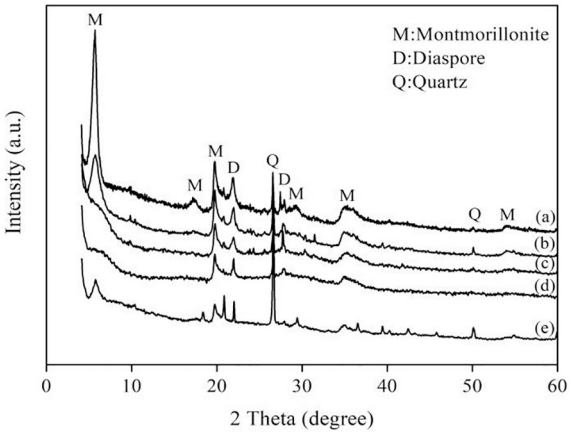

Fig. 1. X-ray diffraction patterns of (a) CaM, (b) Zr-CaM0.1, (c) Zr-CaM0.5, (d) Zr-CaM1 and (e) Phoslock.

The XRD spectra of CaM, as-prepared Zr-CaMs, and Phoslock are presented in Fig. 1. The raw CaM exhibited a strikingly sharp peak centered at 5.71° and a number of weaker peaks at 17.18°, 19.76°, 27.92°, 35.33°, and 54.89°, corresponding to the characteristic montmorillonite crystal structure. Other distinct peaks were attributed to the impurities of the diaspore and quartz (Huang et al., 2015; Lin et al., 2018). Phoslock is typically manufactured by patent using an ion exchange process with a bentonite and La solution (Robb et al., 2003; Haghseresht et al., 2009). Bentonite is a type of clay mineral composed of more than 75% montmorillonite. Hence, Phoslock exhibited a similar XRD pattern, but its peak strength was weak for the impurity, compared to that of the raw CaM. The intensities of most of the peaks decreased after the addition of Zr, although the positions of the major diffraction peaks remain unchanged in the Zr-CaMs. In contrast to the raw CaM, one remarkable peak presented at 5.71°, and two other marginal peaks disappeared at 17.18° and 27.92° for Zr-CaM0.5 and Zr-CaM1, instead of a wider peak occurring near 7°. This peak was attributed to amorphous zirconia (Zong et al., 2016) because of the introduction of the Zr source. Additionally, the basal surface spacing of the raw CaM was 1.59 nm based on the Bragg equation ($2d\sin\theta = n\lambda$), which is slightly less than that of Zr-pillared montmorillonite (1.79 nm) (Huang et al., 2015).

The SEM micrographs of CaM, Zr-CaMs, and Phoslock are shown in Fig. 2. The CaM surface was uneven and porous with large honeycomb-like blocks. The SEM images of Zr-CaM0.1 also appeared non-uniform with adherent block particles, whereas Zr-CaM0.5 and Zr-CaM1 exhibited clear layer stripping and large numbers of small lamellar structures with high dispersities. These Zr-CaMs morphology transformations caused an increase in the SSA and total pore volume. It has been proved that the SSA values were determined to be 173.92 m^2/g and 192.33 m^2/g for Zr-CaM0.5 and Zr-CaM1, respectively, in the following study. Thus, the Zr loaded onto montmorillonite dramatically facilitated its affinity towards phosphate. Huang et al. (2015) found that the SSA and total micropore volume of Zr-pillared montmorillonite were 5 and 17 times larger than those of the pristine montmorillonite, respectively. They further pointed out that Zr primarily entered into the interlayer through cation exchange and then bound with the skeleton, $[Si_4O_{10}]n$, of the raw montmorillonite. The Zr modification did not completely destroy the montmorillonite structure, according to the XRD spectra results, but it contributed to the phosphate adsorption performance due to the increase in the number of active adsorption sites on the surface and inner pore channels. Phoslock displayed similar a SEM micrograph to that of Zr-CaM0.1. In comparison, Phoslock has a smaller SSA, as determined in the present study (Table 1) and previous reports

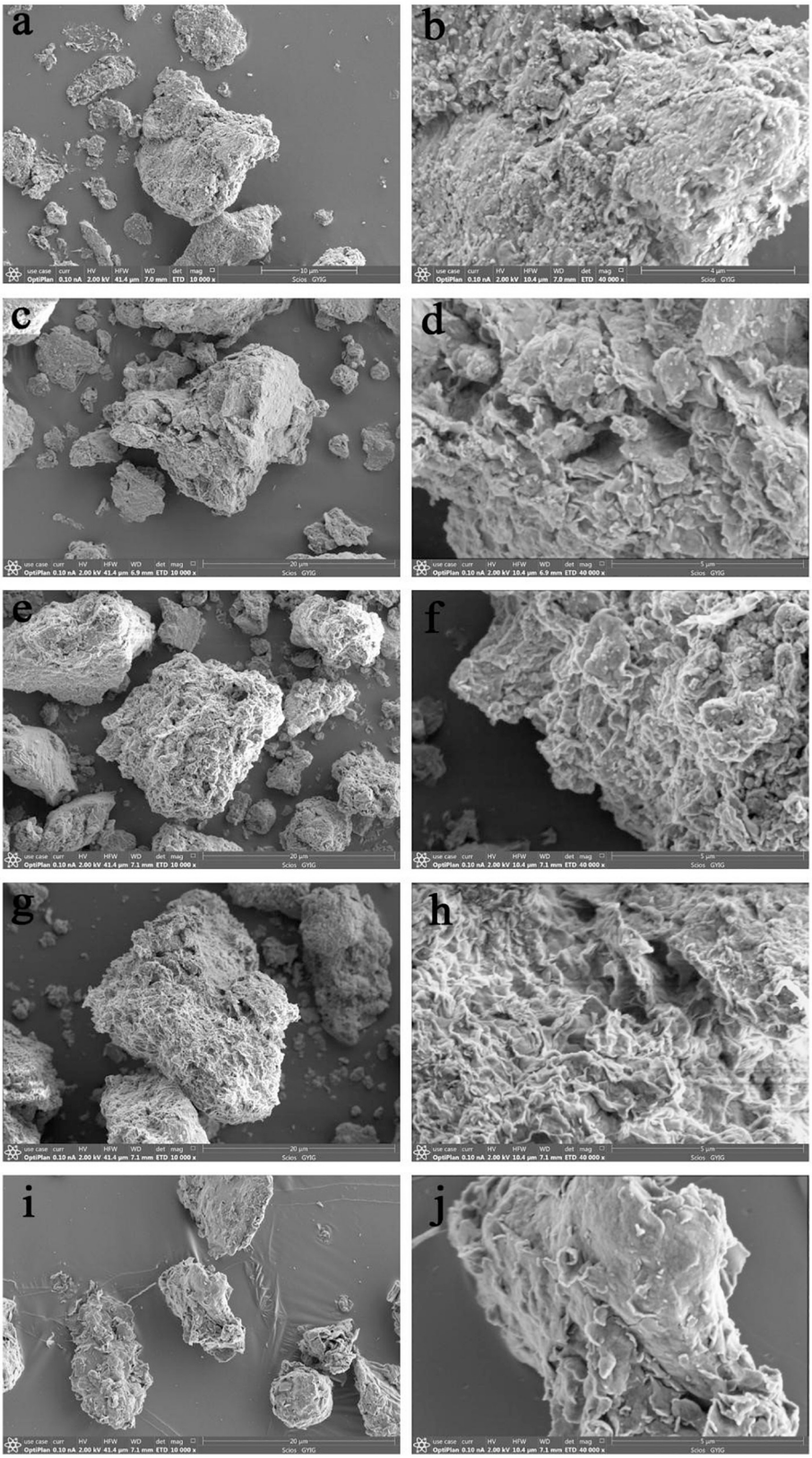

Fig. 2. SEM micrographs of (a, b) CaM, (c, d) Zr-CaM0.1, (e, f) Zr-CaM0.5, (g, h) Zr-CaM1 and (i, j) Phoslock. The micrographs on the left represented 10,000 times magnification, and right parts magnified 40,000 times.

(Haghseresht et al., 2009; Yin et al., 2016), which may constrain its phosphate adsorption capacity from wastewater.

The chemical compositions of CaM, Zr-CaMs, and Phoslock are presented in Table 2. SiO_2, Al_2O_3, MgO, CaO, and Fe_2O_3 were the main components of CaM, with small amounts of Na_2O, K_2O, TiO_2, and MnO. It can be deduced that Mg^{2+} and Ca^{2+} are major exchangeable cations

Table 2
Chemical compositions (wt%) of different materials determined by XRF.

Compounds	CaM	Zr-CaM0.1	Zr-CaM0.5	Zr-CaM1	Phoslock
SiO_2	64.08	52.47	42.12	34.70	63.01
Al_2O_3	15.69	13.28	10.73	9.15	14.90
MgO	4.21	3.84	3.14	2.72	3.16
CaO	2.96	2.32	1.85	1.63	3.07
Fe_2O_3	2.90	2.14	1.73	1.48	3.18
Na_2O	0.55	1.59	1.73	1.80	0.91
K_2O	0.37	0.34	0.26	0.20	1.29
TiO_2	0.23	0.20	0.17	0.15	0.30
MnO	0.06	0.06	0.05	0.04	–
ZrO_2	–	3.71	14.75	26.01	–
Others	0.29	0.26	0.43	0.55	0.17
LOI	8.66	19.79	23.04	21.57	10.01

– below the detect limit.
Others represent some metallic oxides at trace amount.

in the montmorillonite layers. The XRF analysis showed that the relative contents of Si, Al, Mg, Fe, and Ca decreased with an increasing Zr-loading ratio, whereas those of Zr and Na increased. This also indicated that Zr was successfully loaded onto the surface and interlayer of the montmorillonite by exchanging with free Mg^{2+} and Ca^{2+} cations. The Zr-loading rates of Zr-CaM0.1, Zr-CaM0.5, and Zr-CaM1 were approximately 2.74%, 10.91%, and 19.24%, respectively, as calculated from the relative contents of ZrO_2 (Table 2). The increasing proportion of Na was attributed to the intervention during pH regulation. Like CaM, Phoslock was also predominately composed of SiO_2, Al_2O_3, MgO, CaO, and Fe_2O_3, corresponding to the bentonite matrix.

Trace elemental compositions of CaM, Zr-CaMs, and Phoslock were analyzed by ICP-MS, as shown in Table 3. The results also supported that the Zr loading was significantly related to the preparation of Zr-CaMs. Additionally, the Zr content in Phoslock was comparable to that in CaM, whereas the La content was three orders of magnitude higher than that in other materials. As one of the rare earth elements, the dissolution of La from Phoslock is potentially hazardous to benthic infauna, e.g., chironomids, *Daphnia magna*, and dubia (Reitzel et al., 2013b; Copetti et al., 2016). A recent bioaccumulation investigation stated that over 20 μg/L La^{3+} ions are lethal to the hairy marrons, crustaceans, and some other phyla (Svatos, 2018). Previous studies have confirmed that Zr^{4+} did not leak from Zr-modified montmorillonite in a pH range of 3.0–9.0, indicating the sufficient stability and ecological security of the Zr-CaMs (Huang et al., 2015). Moreover, the harm of Zr to aquatic organisms has not been reported on previously.

3.2. Static adsorption of phosphate

The variation trends of phosphate adsorption by CaM, Zr-CaMs, and Phoslock under designed initial P concentration conditions are shown in Fig. 3, with adsorption capacities in the order of Zr-CaM1 > Zr-CaM0.5, Phoslock > Zr-CaM0.1 > CaM. Zr-CaM0.5, Zr-CaM1, and Phoslock, which nearly synchronously reached the adsorption equilibrium after 17 d. CaM had nearly no adsorption effect on the three P-containing solutions due to the small SSA and pore volume (Table 1). The increasing P concentration in the initial experimental stage following the addition of CaM was probably because the montmorillonite particles quickly dispersed after they encountered water and partially released inherent P into the ambient aqueous solution. High Zr loading ratios in Zr-CaM1 have superior phosphate adsorption performance to those of Zr-CaM0.5 and Zr-CaM0.1. For the three types of simulating solutions, the equilibrium concentrations was reduced to 0.014 mg/L, 0.022 mg/L, and 0.046 mg/L after the addition of Zr-CaM1, and

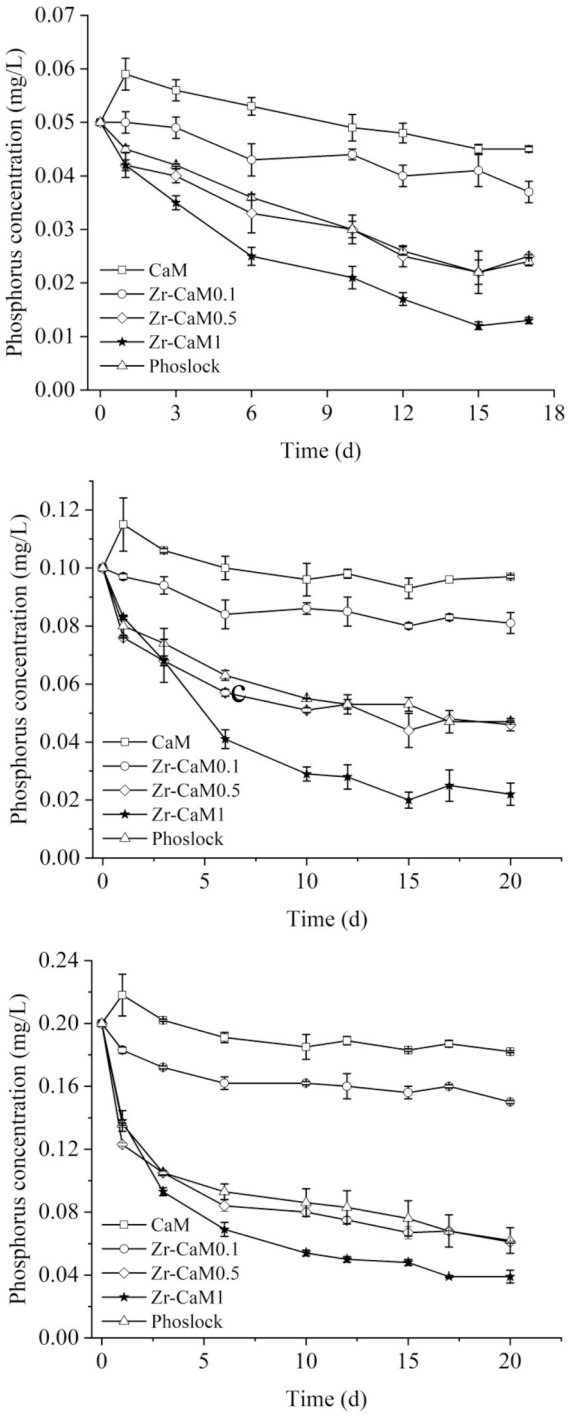

Fig. 3. Static adsorption of phosphate by different adsorbents as a function of contact time. Experimental condition: solution initial P concentration 0.05 mg/L, 0.10 mg/L, and 0.20 mg/L, dosage ratio of 100/1, pH 7 and temperature 298 K.

Table 3
Contents (μg/g) of trace elements in different materials analyzed by ICP-MS.

Elements	CaM	Zr-NM-CaM0.1	Zr-NM-CaM0.5	Zr-NM-CaM1	Phoslock
Zr	140	19968	70440	133455	139
La	33.5	36.1	26.1	26.2	45500
Cr	43.5	51.2	31.6	35.2	22.0
Ni	10.9	12.9	8.52	8.29	11.7
Cu	7.00	8.99	6.28	6.53	24.7
Zn	46.3	45.1	35.3	38.7	75.3
As	3.46	4.11	1.07	0.97	5.18
Cd	0.27	0.34	0.87	1.59	0.32
Pb	26.2	29.0	20.8	24.3	28.5

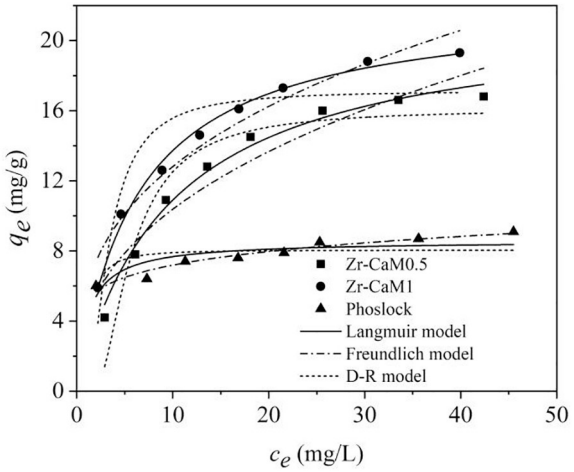

Fig. 4. Isotherms of phosphate adsorption by Zr-CaM0.5, Zr-CaM1, and Phoslock.
The experimental data and predicted curves of the adsorption capacities at equilibrium fitted by nonlinear regression of Langmuir, Freundlich, and D–R models.

0.026 mg/L, 0.047 mg/L, and 0.062 mg/L after the addition of Phoslock. As a result, the removal rates of P by Zr-CaM1 exceeded 72%, which were higher compared to those of Phoslock (48–69%). Reports have pointed out that Phoslock is far from satisfactory for controlling P in low concentrations in field tests, especially that below 0.05 mg/L (Moss et al., 2014; Dithmer et al., 2016). Thus, Phoslock has been recommended to be repeatedly dosed in certain field studies to guarantee phosphate removal and algal bloom inhibition (Moss et al., 2014; Copetti et al., 2016).

3.3. Adsorption isotherms

The adsorption isotherms of Zr-CaM0.5, Zr-CaM1, and Phoslock were investigated; the results are shown in Fig. 4, and the corresponding parameters and R^2, *MRE*, and Δq values are provided in Table 4. The R^2 obtained from the Langmuir model for Zr-CaM0.5 and Zr-CaM1 were the highest of the three models. Additionally, *MRE* and Δq were determined to quantitatively compare the model applicabilities. Based on the results of the nonlinear plot (Fig. 4 and Table 4), the Langmuir model sufficiently described the adsorption data with the lowest *MRE* values of 1.656% and 0.256% for Zr-CaM0.5 and Zr-CaM1, respectively. The $q_{e,cal}$ calculated from this model was closer to $q_{e,exp}$, resulting in a lower Δq. Accordingly, the phosphate adsorption by Zr-CaMs can act as homogeneous monolayer coverage. These findings were similar to those of previous reports that used other Zr-modified adsorbents (Huang et al., 2015; Lin et al., 2018). However, unlike that of Zr-CaMs, the better fit of the Freundlich model to the experimental data suggested that phosphate adsorption by Phoslock occurred on the heterogeneous composite surface. The maximum adsorption capacities of Zr-CaM1, Zr-CaM0.5, and Phoslock via the Langmuir nonlinear model were 22.37 mg/g, 21.53 mg/g, and 8.58 mg/g, respectively. The value of K_L also decreased in the same order.

The phosphate adsorption performances of Zr-related adsorbents in the literature are summarized in Table 5, including those of zirconia hydrate (Rodrigues et al., 2012), mesoporous zirconia (Liu et al., 2008), amorphous nano-zirconia (Su et al., 2013), Zr-modified zeolite (Zhan et al., 2017), Zr-modified bentonite (Lin et al., 2018), and Zr/Al-pillared montmorillonite (Huang et al., 2015). Clearly, the adsorption capacities of Zr-CaM0.5 and Zr-CaM1 prepared in this study were superior to those of the other Zr-modified aluminosilicate minerals and were slightly lower than those of the Zr based oxides, such as mesoporous zirconia and amorphous nano-zirconia.

3.4. Adsorption kinetics

The phosphate adsorption capacities of Zr-CaM0.5 and Zr-CaM1 as a function of reaction time and their adsorption kinetics fits are shown in Fig. 5a and Table 6. The pseudo-second-order model exhibited a higher R^2 and a lower *MRE* and Δq than those of the pseudo-first-order model; however, the Elovich model best fit the experimental data, particularly for Zr-CaM0.5. This further supported that the observed adsorption feature may be a chemisorption process, which agreed with the isotherm results described above.

The entire adsorption process can be divided into three distinctive stages (Fig. 5b). The first stage is rapid adsorption on the Zr-CaM0.5 and Zr-CaM1 surface within the initial 12 h, and then it slowed during the next 12–36 h in the second stage, and the adsorption reached equilibrium around the third day. For the 0.20 mg/L P solution, over half of the phosphate was absorbed by Zr-CaM1 within the initial 3 h. This excellent removal rate was because of the rapid membrane diffusion of phosphate to the active sites on the adsorbent surface (Lin et al., 2018). Afterwards, the active point decreased with an increased reaction time, resulting in the slower adsorption rate. After 72 h, the sorption process reached equilibrium, and the remaining P concentration was reduced by 0.02 mg/L, corresponding to the TP threshold of Class II surface water for China within the safe water quality standard.

3.5. Influencing factors

3.5.1. Effect of adsorbent dosage

Zr-CaM1 was selected for the dosage test of Zr-CaMs for phosphate adsorption. The adsorption capacities varied with different dosages and are shown in Fig. 6. The adsorption rate of phosphate increased from 16.8% to 92.3%, while the adsorption capacity decreased by 50%, when the Zr-CaM1 dosage increased from 0.004 g/L to 0.04 g/L. This was because the unsaturated sites on the adsorbent surface increased with the addition of Zr-CaM1, whereas the unit adsorption capacity decreased. Considering the cost and the adsorption performance of Zr-CaM1, the optimum dosage, from 100/1 to 150/1, is recommended for practical applications for phosphate removal from surface water with low P concentrations. This ratio is roughly the same as that of Phoslock (Reitzel et al., 2013a).

3.5.2. pH effect on phosphate adsorption

The phosphate adsorption capacity of Zr-CaM1 changed with different solution pHs as shown in Fig. 7. Remarkably, the adsorption performance of Zr-CaM1 fluctuated marginally in the range of

Table 4
Adsorption isotherm parameters for phosphate adsorption by Zr-CaM0.5, Zr-CaM1, and Phoslock calculated from nonlinear models.

Adsorbent	Langmuir					Freundlich					Dubinin-Radushkevich				
	q_m (mg/g)	K_L (L/mg)	R^2	*MRE* (%)	Δq	K_F ((mg$^{(1-1/n)}$L$^{1/n}$)/g)	$1/n$	R^2	*MRE* (%)	Δq	q_{DR} (mmol /g)	K_{DR} (mol^2/kJ^2)	R^2	*MRE* (%)	Δq
Zr-CaM0.5	21.53	0.102	0.984	1.656	0.076	4.15	0.398	0.901	4.051	0.210	16.09	4.68×10^{-6}	0.894	5.089	0.264
Zr-CaM1	22.37	0.161	0.993	0.256	0.031	5.84	0.342	0.951	1.771	0.118	17.14	1.78×10^{-6}	0.812	1.230	0.175
Phoslock	8.58	0.084	0.650	0.219	0.085	5.11	0.148	0.936	0.032	0.038	8.05	3.38×10^{-7}	0.409	0.675	0.106

Table 5
Summary of maximum phosphate adsorption capacities of Zr-CaMs and other Zr-related adsorbents reported in the literature.

Adsorbent	Initial phosphate concentration (mg/L)	Adsorption capacity (mg/g)	Ref.
Mesoporous ZrO_2	0–300	29.71	Liu et al., 2008
Hydrous zirconium oxide	100–150	53	Rodrigues et al., 2012
Amorphous zirconium oxide nanoparticles	5–50	99.01	Su et al., 2013
Zr-modified zeolite	0.2–4	5.96	Zhan et al., 2017
Zr-modified Ca^{2+}-pretreated bentonite	2–35	13.4	Lin et al., 2018
Zr-pillared montmorillonite	20–50	13.1	Huang et al., 2015
Zr/Al-pillared montmorillonite	20–50	17.2	Huang et al., 2015
Zr-CaM0.5	1–50	21.53	This study
Zr-CaM1	1–50	22.37	This study

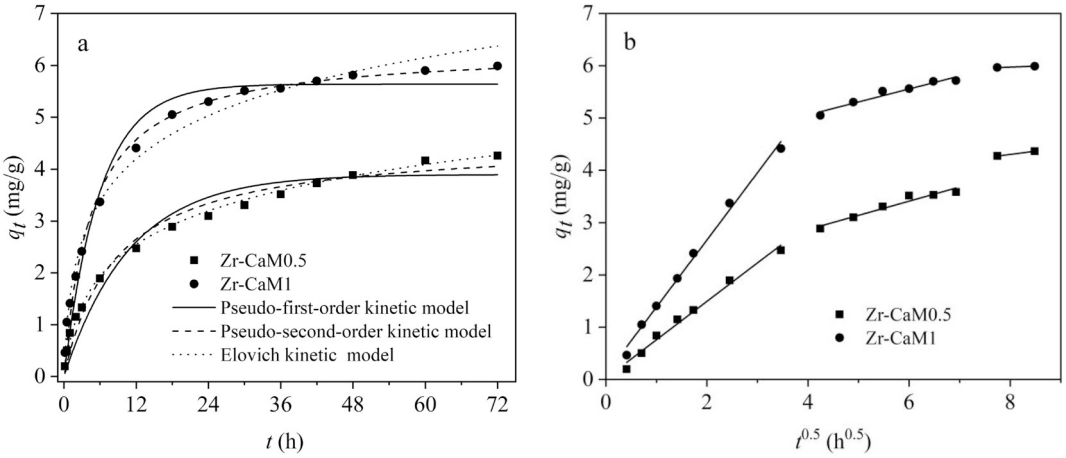

Fig. 5. Kinetics of phosphate adsorption by Zr-CaM0.5 and Zr-CaM1 fitted by (a) pseudo-first-order, pseudo-second-order, and Elovich kinetic nonlinear models, (b) Three adsorption stages differentiated by an intra-particle diffusion linear model.

4.61–5.20 mg/g at the adsorption equilibrium when the solution pH increased from 4 to 8.5. However, it dramatically dropped to 3.66 mg/g at a pH of 10.0. It is well-known that the form of phosphate depends on the solution pH. The ionization constants (p*K*a) of $H_2PO_4^-$, HPO_4^{2-}, and PO_4^{3-} are 2.16, 7.20, and 10.30, respectively (Haghseresht et al., 2009). When the pH value of the aqueous solution varied from 4 to 8.5, the relative proportion of $H_2PO_4^-$ diminished gradually following an elevated contribution of HPO_4^{2-}. Many researchers have demonstrated that $H_2PO_4^-$ is more vulnerable to coordination exchange than HPO_4^{2-} and is subsequently adsorbed by the Zr-based adsorbents (Su et al., 2013; Huang et al., 2015). When further increasing the solution pH, the Zr-CaM1 surface becomes more negatively charged. Hydroxide ions compete with phosphate for the effective adsorption sites on the adsorbent. Relevant studies have pointed out that the adsorption capacities of Zr/Al-modified montmorillonite and Zr-modified bentonite are strongly pH-dependent, and they are reduced by 36–56% and 50–64% from pH 4 to 10, respectively (Huang et al., 2015; Lin et al., 2018). Phoslock was also affected by the pH restrictions of the solution (Ross et al., 2008; Haghseresht et al., 2009; Zamparas et al., 2015). Therefore, Zr-CaM1 had a wide pH range compatibility for phosphate removal from natural water.

3.5.3. Effect of the coexisting anions

The impacts of SO_4^{2-}, Cl^-, and HCO_3^- on phosphate adsorption onto Zr-CaM1 are presented in Fig. 8. When the HCO_3^- concentration of the aqueous solution increased from 0 mmol/L to 3.3 mmol/L, the phosphate adsorption capacity decreased from 4.26 mg/g to 2.32 mg/g, indicating a great inhibiting effect. In contrast, the presence of Cl^- and SO_4^{2-} can promote the adsorption process. HCO_3^- is extensive in surface waters, as an important component of water alkalinity (Han and Liu, 2004; Li et al., 2019). It can elevate the initial solution pH and interfere with phosphate adsorption (Tian et al., 2009; Huang et al., 2015). HCO_3^- and CO_3^{2-} also exerted a substantial influence on the phosphate adsorption by Phoslock (Reitzel et al., 2013a; Dithmer et al., 2016). In addition to HCO_3^-, Cl^- and SO_4^{2-} can increase ionic strength, further improving the affinity of Zr-CaM1 towards phosphate, which is similar to previous reports on Zr-modified Ca-based bentonite (Lin et al., 2018).

3.6. Proposed mechanisms for phosphate adsorption onto Zr-CaMs

Significant effort has been undertaken to unravel the removal mechanism of phosphate by Zr-modified clay minerals (Huang et al., 2015; Lin et al., 2018; Wu et al., 2020). Two major mechanisms are proposed for phosphate removal by these adsorbents: electrostatic attraction and inner sphere complex formation (Lin et al., 2018; Wu et al., 2020). The surface charge of an adsorbent is highly dependent on the solution pH. When the solution pH is lower than pH_{PZC} (pH at the point of zero charge), then the adsorbent surface is positively charged. However, when the solution pH is higher than pH_{PZC}, the adsorbent surface carries a net negative charge. It was speculated that the pH_{PZC} of Zr-CaMs exceeds 7.0 based on a previous investigation of a similar Zr-modified zeolite (pH_{PZC} = 8.0, Zhan et al., 2017) and bentonite (pH_{PZC} = 7.83, Lin et al., 2018). This may indicate that the Zr-CaMs were positively charged by the protonation of surface hydroxyl groups at a solution pH of 7. In this case, the adsorption of phosphate by Zr-CaMs may be achieved through electrostatic attraction. However, because the phosphate adsorption in this study is a chemisorption-dominated process (based on the adsorption isotherms and kinetics studies), the contribution of the purely electrostatic attraction mechanism to the phosphate adsorption appears insignificant.

In this study, Zr was introduced to the surface and interlayer of raw CaM, as supported by the results of both the XRF and ICP-MS (Tables 2 and 3). This introduction also dramatically changed the surface

Table 6
Kinetic parameters for phosphate adsorption by Zr-CaM0.5 and Zr-CaM1 calculated via nonlinear models, except an intra-particle diffusion model.

Adsorbent	Pseudo-first-order model					Pseudo-second-order model					Elovich model					Intra-particle diffusion model		
	q_e (mg/g)	k_1 (1/h)	R^2	*MRE* (%)	Δq	q_e (mg/g)	k_2 (g/ mg h)	R^2	*MRE* (%)	Δq	*a* (mg/(g h))	β (g/mg)	R^2	*MRE* (%)	Δq	K_i (mg/g $h^{0.5}$)	C_i (mg/g)	R^2
Zr-CaM0.5	3.890	0.091	0.938	17.19	0.341	4.538	0.026	0.975	11.32	0.248	0.983	1.005	0.996	3.83	0.101	0.508	0.357	0.965
Zr-CaM1	5.639	0.167	0.970	11.42	0.263	6.321	0.034	0.992	6.83	0.184	3.012	0.815	0.991	0.28	0.063	0.736	0.911	0.903

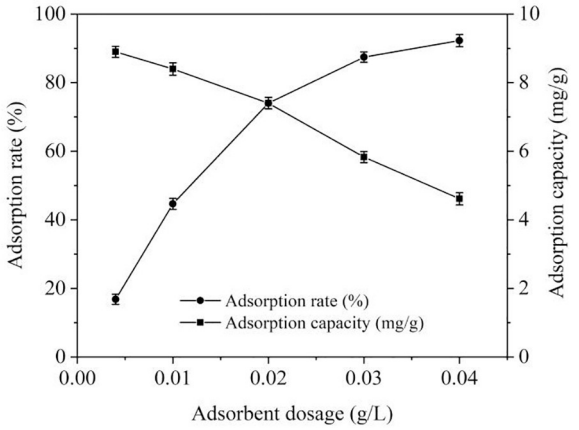

Fig. 6. Effect of different Zr-CaM1dosages on the adsorption rate of phosphate.

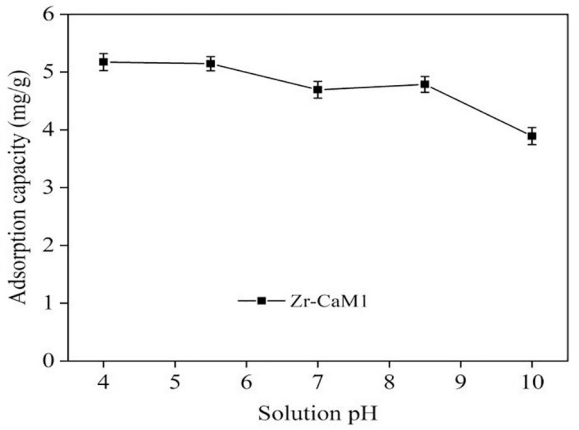

Fig. 7. Effect of solution pH on the phosphate adsorption capacity of Zr-CaM1.

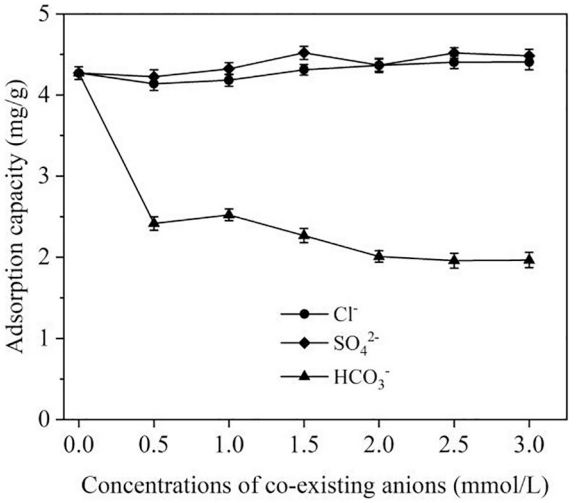

Fig. 8. Effect of the co-existing anions on the phosphate adsorption capacity of Zr-CaM1.

morphologies and microporous structures of Zr-CaMs, especially for Zr-CaM0.5 and Zr-CaM1, which was evident from the XRD and SEM characterization (Figs. 1 and 2), thus improving their phosphate adsorption capacities.

It has been proven that Zr^{4+} can be combined with the silicon-oxygen tetrahedron of montmorillonite in the presence a stable [Si—O]…[HO—Zr] hydrogen bond (Huang et al., 2015). Previous studies

confirmed that Zr-modified montmorillonite has a sufficient affinity towards phosphate through the replacement of hydroxyl groups (≡ZrOH) on the adsorbent surface and the subsequent formation of mononuclear monodentate and binuclear bidentate inner-sphere complexes (Su et al., 2013; Huang et al., 2015; Wu et al., 2020). These processes can be explained as Eqs. (4)–(6).

$$\equiv Zr\blacksquare OH + H_2PO_4^- = \equiv Zr\blacksquare(H_2PO_4) + OH^- \quad (4)$$

$$\equiv Zr\blacksquare OH + HPO_4^{2-} = \equiv Zr\blacksquare(HPO_4)^- + OH^- \quad (5)$$

$$2(\equiv Zr\blacksquare OH) + HPO_4^{2-} = \equiv Zr_2\blacksquare(HPO_4) + 2OH^- \quad (6)$$

4. Conclusion

This study demonstrated that Zr was successfully loaded onto the surface and interlayer of CaM by the addition of $ZrOCl_2{\cdot}8H_2O$, thus greatly facilitating the removal efficiency of phosphate. The adsorption isotherm fit the Langmuir model better than the Freundlich and D-R models. The maximum P adsorption capacities of Zr-CaM0.5 and Zr-CaM1 obtained from the Langmuir nonlinear model reached 21.53 mg/g and 22.37 mg/g, which were significantly higher than those of Phoslock and ZrCaBT. The kinetics behavior agreed with the Elovich kinetic model results, suggesting a chemical adsorption process. The mechanism for phosphate adsorption by Zr-CaMs was largely ascribed to the ligand exchange of surface hydroxyl groups with phosphate. Moreover, Zr-CaM1 had a wide pH range (4–8.5) applicability for phosphate adsorption performance and thus can be considered a highly effective, economic, and environmentally safe adsorbent for phosphate removal from contaminated surface water, especially for ultralow P concentrations.

Declaration of Competing Interest

The authors declare that they have no known competing financial interests or personal relationships that could have appeared to influence the work reported in this paper.

Acknowledgement

This study was supported by the National Natural Science Foundation of China (No. 41573133, U1612442) and Opening Fund of the State Key Laboratory of Environmental Geochemistry (No. SKLEG2018909). The two anonymous reviewers are particularly appreciated for their valuable comments that greatly improved the manuscript. We also thank the Elsevier Author Services for the assistance in language editing.

Appendix A. Supplementary data

Supplementary data to this article can be found online at https://doi.org/10.1016/j.clay.2020.105638.

References

American Public Health Association, A.W.W.A, Water Environmental Federation, 2017. Standard Methods for the Examination of Water and Wastewater, 23rd Edition. In: American Public Health Association (APHA). American Public Health Association, Washington, DC, USA.
Borgnino, L., Avena, M.J., De Pauli, C.P., 2009. Synthesis and characterization of Fe(III)-montmorillonites for phosphate adsorption. Colloid Surf. A. 341, 46–52.
Chitrakar, R., Tezuka, S., Sonoda, A., 2006. Selective adsorption of phosphate from seawater and wastewater by amorphous zirconium hydroxide. J. Colloid Interface Sci. 297, 426–433.
Choi, J., Chung, J., Lee, W., Kim, J.O., 2016. Phosphorous adsorption on synthesized magnetite in wastewater. J. Ind. Eng. Chem. 34, 198–203.
Copetti, D., Finsterle, K., Marziali, L., Stefani, F., Tartari, G., Douglas, G., Reitzel, K., Spears, B.M., Winfield, I.J., Crosa, G., D'Hase, P., Yasseri, S., Lürling, M., 2016. Eutrophication management in surface waters using lanthanum modified bentonite: a review. Water Res. 97, 162–174.
D'Haese, P.C., Douglas, G., Verhulst, A., Neven, E., Behets, G.J., Vervaet, B.A., Finsterle, K., Lürling, M., Spears, B., 2019. Human health risk associated with the management of phosphorus in freshwaters using lanthanum and aluminium. Chemosphere 220, 286–299.
Dithmer, L., Nielsen, U.G., Lürling, M., Spears, B.M., Yasseri, S., Lundberg, D., Moore, A., Jensen, N.D., Reitzel, K., 2016. Responses in sediment phosphorus and lanthanum concentrations and composition across 10 lakes following applications of lanthanum modified bentonite. Water Res. 97, 101–110.
Environmental Quality Standard for Surface Water (EQSSW), 2002. Ministry of Environmental Protection of P. R. China, Beijing.
Freundlich, H., 1926. Colloid and Capillary Chemistry. Methuen, London.
Gan, F., Luo, Y., Hang, X., Zhao, H., 2016. Heterocoagulated clay-derived adsorbents for phosphate decontamination from aqueous solution. J. Environ. Manag. 166, 23–30.
Haghseresht, F., Wang, S., Do, D.D., 2009. A novel lanthanum-modified bentonite, Phoslock, for phosphate removal from wastewaters. Appl. Clay Sci. 46, 369–375.
Han, G., Liu, C., 2004. Water geochemistry controlled by carbonate dissolution: a study of the river waters draining karst-dominated terrain, Guizhou Province. China. Chem. Geol. 204, 1–21.
Heathwaite, L., Sharpley, A., 1999. Evaluating measures to control the impact of agricultural phosphorus on water quality. Water Sci. Technol. 39, 149–155.
Ho, Y.S., McKay, G., 1999. Pseudo-second order model for sorption processes. Process Biochem. 34, 451–465.
Huang, W., Chen, J., He, F., 2015. Effective phosphate adsorption by Zr/Al-pillared montmorillonite: insight into equilibrium, kinetics and thermodynamics. Appl. Clay Sci. 104, 252–260.
Koppelaar, R.H.E.M., Weikard, H.P., 2013. Assessing phosphate rock depletion and phosphorus recycling options. Glob. Environ. Chang. 23, 1454–1466.
Langmuir, I., 1916. The constitution and fundamental properties of solids and liquids part I. Solid. J. Am. Chem. Soc. 38, 2221–2295.
Li, H., Wang, S., Bai, X., Cao, Y., Wu, L., 2019. Spatiotemporal evolution of carbon sequestration of limestone weathering in China. Sci. China Earth Sci. 62, 974–991.
Lin, J., Jiang, B., Zhan, Y., 2018. Effect of pre-treatment of bentonite with sodium and calcium ions on phosphate adsorption onto zirconium-modified bentonite. J. Environ. Manag. 217, 183–195.
Liu, H., Sun, X., Yin, C., 2008. Removal of phosphate by mesoporous ZrO_2. J. Hazard. Mater. 151, 616–622.
Loganathan, P., Vigneswaran, S., Kandasamy, J., Bolan, N.S., 2014. Removal and recovery of phosphate from water using sorption. Crit. Rev. Environ. Sci. Technol. 44, 847–907.
Maavara, T., Parsons, C.T., Ridenour, C., Stojanovic, S., Dürr, H.H., Powley, H.R., Van, C.P., 2015. Global phosphorus retention by river damming. Proc. Natl. Acad. Sci. U. S. A. 112, 15603–15608.
Marquez-Pacheco, H., Hansen, A.M., Falcon-Rojas, A., 2013. Phosphorous control in a eutrophied reservoir. Environ. Sci. Pollut. Res. 20, 8446–8456.
Moss, M.T., Taffs, K.H., Longstaff, B.J., Ginn, B.K., 2014. Establishing ecological reference conditions and tracking post-application effectiveness of lanthanum saturated bentonite clay (Phoslock®) for reducing phosphorous in aquatic ecosystems: an applied paleolimnological approach. J. Environ. Manag. 141, 77–85.
Pandey, S., 2017. A comprehensive review on recent developments in bentonite-based materials used as adsorbents for wastewater treatment. J. Mol. Liq. 241, 1091–1113.
Peñuelas, J., Sardans, J., Rivas-Ubach, A., Janssens, I., 2012. The human-induced imbalance between C, N and P in Earth's life system. Glob. Chang. Biol. 18, 3–6.
Reitzel, K., Andersen, F.Ø., Egemose, S., Jensen, H.S., 2013a. Phosphate adsorption by lanthanum modified bentonite clay in fresh and brackish water. Water Res. 47, 2787–2796.
Reitzel, K., Lotter, S., Dubke, M., Egemose, S., Jensen, H.S., Andersen, F.Ø., 2013b. Effects of Phoslock_treatment and chironomids on the exchange of nutrients between sediment and water. Hydrobiologia 703, 189–202.
Robb, M., Greenop, B., Goss, Z., Douglas, G., Adeney, J., 2003. Application of Phoslock®, an innovative phosphorus binding clay, to two Western Australian waterways: preliminary findings. Hydrobiologia 494, 237–243.
Rodrigues, L.A., Leandro, J.M., Coppio, L.D.S.C., 2012. Adsorption of phosphate from aqueous solution by hydrous zirconium oxide. Environ. Technol. 33, 1345–1351.
Ross, G., Haghseresht, F., Cloete, T.E., 2008. The effect of pH and anoxia on the performance of Phoslock®, a phosphorus binding clay. Harmful Algae 7, 545–550.
Ruban, V., López-Sánchez, J.F., Pardo, P., Rauret, G., Muntau, H., Quevauviller, P., 2001. Harmonized protocol and certified reference material for the determination of extractable contents of phosphorus in freshwater sediments a synthesis of recent works. Fresenius J. Anal. Chem. 370, 224–228.
Smil, V., 2000. Phosphorus in the environment: Natural flows and human interferences. Annu. Rev. Energy Environ. 25, 53–88.
Spears, B.M., Lürling, M., Yasseri, S., Castro-Castellon, A.T., Gibbs, M., Meis, S., McDonald, C., McIntosh, J., Sleep, D., Van Oosterhout, F., 2013. Lake responses following lanthanum-modified bentonite clay (Phoslock®) application: an analysis of water column lanthanum data from 16 case study lakes. Water Res. 47, 5930–5942.
Su, Y., Cui, H., Li, Q., 2013. Strong adsorption of phosphate by amorphous zirconium oxide nanoparticles. Water Res. 47, 5018–5026.
Svatos, K.B.W., 2018. Commercial silicate phosphate sequestration and desorption leads to a gradual decline of aquatic systems. Environ. Sci. Pollut. Res. 25, 5386–5392.
Tian, S., Jiang, P., Ning, P., Su, Y., 2009. Enhanced adsorption removal of phosphate from water by mixed lanthanum/aluminum pillared montmorillonite. Chem. Eng. J. 151, 141–148.
Wendling, L.A., Blomberg, P., Sarlin, T., Priha, O., Arnold, M., 2013. Phosphorus sorption and recovery using mineral-based materials: Sorption mechanisms and potential phytoavailability. Appl. Geochem. 37, 157–169.

Wu, B., Wan, J., Zhang, Y., Pan, B., Lo, I., 2020. Selective Phosphate Removal from Water and Wastewater using Sorption: Process Fundamentals and Removal Mechanisms. Environ. Sci. Technol. 54, 50–66.
Yamanaka, S., Brindley, G.W., 1979. High surface area solids obtained by reaction of montmorillonite with zirconyl chloride. Clay Clay Miner. 27, 119–124.
Yazdani, M., Bhatnagar, A., Vahala, R., 2017. Synthesis, characterization and exploitation of nano-TiO2/feldsparembedded chitosan beads towards UV-assisted adsorptive abatement of aqueous arsenic (As). Chem. Eng. J. 316, 370–382.
Yin, H., Kong, M., Han, M., Fan, C., 2016. Influence of sediment resuspension on the efficacy of geoengineering materials in the control of internal phosphorous loading from shallow eutrophic lakes. Environ. Pollut. 219, 568–579.
Zamparas, M., Gavriil, G., Coutelieris, F.A., Zacharias, I., 2015. A theoretical and experimental study on the P-adsorption capacity of Phoslock™. Appl. Clay Sci. 335, 147–152.
Zhan, Y., Zhang, H., Lin, J., Zhang, Z., Gao, J., 2017. Role of zeolite's exchangeable cations in phosphate adsorption ontozirconium-modified zeolite. J. Mol. Liq. 243, 624–637.
Zhang, N., Zhao, H., Li, Y., 1990. Research Methods of Clay Minerals. China Science Press, Beijing.
Zong, E., Liu, X., Jiang, J., 2016. Preparation and characterization of zirconia-loaded lignocellulosic butanol residue as a biosorbent for phosphate removal from aqueous solution. Appl. Clay Sci. 387, 419–430.